Seismic Performance of Variable Frequency Pendulum Isolator under Bi-Directional Near-Fault Ground Motions

V.R. Panchal[1] and D.P. Soni[2*]

1. Professor, Dept. of Civil Engineering, Sardar Vallabhbhai Patel Institute of Technology, Vasad-388 306, Gujarat, India
2. Assistant Professor, Dept. of Civil Engineering, Sardar Vallabhbhai Patel Institute of Technology, Vasad-388 306, Gujarat, India,
* Corresponding Author; email: soni_svit@yahoo.com

ABSTRACT

The dynamic response of flexible five-story building supported on the variable frequency pendulum isolator (VFPI) under bi-directional near-fault ground motions is investigated. In order to verify the effectiveness of the VFPI, the seismic responses are compared with the friction pendulum system (FPS) and variable friction pendulum system (VFPS). The response of the system with bi-directional interaction is compared with those without interaction in order to investigate the effects of bi-directional interaction of frictional forces. Moreover, a parametric study is carried out to critically examine the influence of important parameters on bi-directional interaction of the frictional forces of the VFPI. From the above investigations, it is concluded that under bi-directional near-fault ground motions, the isolator displacement in the VFPI is more than that of the VFPS and the FPS whereas the top floor absolute acceleration and the base shear are less than that of the VFPS and the FPS. Furthermore, if the bi-directional interactions of frictional forces of the VFPI are ignored, the isolator displacements will be under predicted and superstructure acceleration and base shear will be over predicted.

Keywords:
Base isolation; Superstructure flexibility; Near-fault ground motions; Bi-directional interaction; VFPI; VFPS

1. Introduction

Recent years have seen a number of catastrophic failures of structures due to severe, impulsive, seismic events such as the 1994 Northridge earthquake in California, the 1995 Kobe earthquake in Japan and 1999 Chi-Chi earthquake in Taiwan. Failure of structures during such events seriously hampers the relief and rehabilitation work. The effect of severe and impulsive earthquakes on the structures has recently received much attention and become a significant concern for reliable aseismic structural design. To protect structures from earthquake damages, seismic isolation technology has been applied over the last three decades. This technology is one of the most widely implemented and accepted technologies for seismic hazard mitigation. The fundamental concept in isolation is to reduce the fundamental frequency of structural vibration to a value lower than the predominant energy-containing frequencies of the earthquake. The other purpose of an isolation system is to provide a mean of energy dissipation, which dissipates the seismic energy transmitted to the system. The goal is to reduce interstory drifts and floor accelerations to limit damage to the structure and its contents in a cost-effective manner.

In spite of the direct benefits of the seismic isolation technology, it has been suggested that the base-isolated buildings can be vulnerable to large pulse-like ground motions generated at near-fault locations [1-2]. Besides Hall et al [1] and Heaton et al [2], several other researchers have also warned about the vulnerability of base-isolated structures to near-fault ground motions (for example [3-4]). Such ground motions can be quite different than those from the far-fault events. In particular, near-fault ground motion records (also known as "epicentral

acceleration records") can contain large long-period spectral components in the fault normal direction, large short-period spectral components in the fault parallel direction and long-duration pulses of ground displacement and high peak ground velocities [5]. These higher spectral inputs, occurring in the neighborhood of important structural periods, can result in a structural response significantly greater than that would occur for a typical far-fault design level event. This concern has influenced the seismic isolation design requirements in the Uniform Building Code, 1997 [6]. In the earlier code there were no near-fault effects but in the recent code, near-fault effects, viz. source type and distance dependent near-fault factors to the customary design spectrum have been introduced. However, it is believed that these factors are not sufficient to solve the problem consistently, because they pay little attention to the physical characteristics of near-fault ground motions. Another concern is a lack of data concerning the behaviour of base-isolated buildings subjected to near-fault ground motions as previous studies have focused mainly on the seismic behavior of base-isolated buildings far from active earthquake faults. Consequently, the effects of these motions on buildings are not yet understood fully.

Among various base isolation systems, the sliding bearings are most popular due to its effectiveness over a wide range of frequency input. The other advantage of sliding bearings is that it ensures the maximum acceleration transmissibility equal to the maximum limiting frictional force. There had been important studies on the efficiency of a variety of sliding bearings by many researchers [7-12]. Most of the above studies on sliding isolation systems are based on the two-dimensional (2-D) planar model of the isolated structure subjected to uni-directional excitation. Such a model of the isolated structures ignores the bi-directional interaction effects of the frictional forces mobilized in the isolation system in two horizontal directions. The bi-directional interaction can play crucial role in the seismic response of structures isolated with the sliding systems. Therefore, it has received much attention and become a significant concern for reliable aseismic design of sliding structures. The recognition of this fact has led several researchers to focus their study on investigating the effects of bi-directional interaction of frictional forces on the response of the structures isolated with sliding systems [13-19]. The review presented so far clearly shows that there have not been many attempts to investigate the behaviour of structures isolated with friction base isolators, especially under bi-directional near-fault ground motions. In view of the above, numerical studies are carried out to understand the behaviour of structures isolated with the *VFPI* under bi-directional near-fault ground motions.

Presented in the paper is the response of five-story building (considering flexible) isolated by the *VFPI* which is investigated under bi-directional near-fault ground motions. The specific objectives of the study are summarized as follows:

i) To demonstrate a method for dynamic analysis of five-story building supported on the *VFPI* by duly incorporating the interaction effects of the frictional forces of the *VFPI*;
ii) To compare the seismic response of building isolated with the *VFPI*, *FPS* and *VFPS* in order to measure the effectiveness of the *VFPI* under bi-directional near-fault ground motions;
iii) To carry out a parametric study with a view to investigate the influence of important parameters on bi-directional interaction effects of frictional forces of the *VFPI*. The important parameters considered are superstructure time period, frequency variation factor (*FVF*) and friction coefficient of the *VFPI*; and
iv) To investigate the effects of bi-directional interaction of friction forces of the *VFPI* on the response of the building under near-fault ground motions (by comparing the response of the system with and without interaction).

2. Variable Frequency Pendulum Isolator

A new isolator called the *VFPI* [20] incorporates the advantages of both the friction pendulum system (*FPS*) and Pure-Friction (*P-F*) isolators, see Figure (1). In this isolator, the shape of the sliding surface is non-spherical. To be more specific, its geometry has been derived from the basic equation of an ellipse, with its semi-major axis being a linear function of sliding displacement. This is equivalent to an infinite number of ellipses continuously transforming into one another such that the semi-major axis is larger for larger sliding displacement. The performance of the *VFPI* is found to be very effective for a variety of excitation and structural characteristics. The *VFPI*

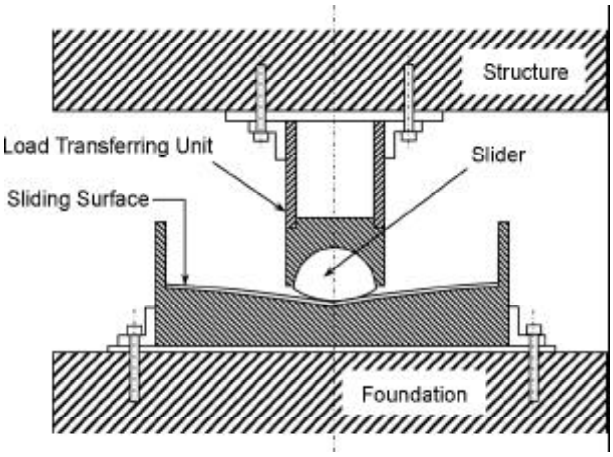

Figure 1. Details of the VFPI [20].

is relatively flatter than the *FPS*, which results in smaller vertical displacement for similar displacements. This is an additional advantage of the *VFPI* compared to the *FPS* since flatter sliding surface will result in the generation of smaller overturning forces in the structure. The most important properties of this system are: i) Its time period of oscillation depends on sliding displacement and ii) Its restoring force exhibits softening behaviour. The isolator geometry is such that its frequency decreases with an increase in sliding displacement and asymptotically approaches zero at very large displacement. As a result, the dominant frequency of excitation and the isolator frequency are not likely to tune. The response of structure with the *FPS* increases for higher time periods, whereas the response of the *VFPI* is almost independent of the structural time period.

The restoring forces of the *VFPI* in the *x*- and *y*-directions are expressed by

$$\begin{Bmatrix} F_{bx} \\ F_{by} \end{Bmatrix} = \begin{Bmatrix} F_x \\ F_y \end{Bmatrix} + \begin{bmatrix} k_b(z_b) & 0 \\ 0 & k_b(z_b) \end{bmatrix} \begin{Bmatrix} x_b \\ y_b \end{Bmatrix} \tag{1}$$

where F_x and F_y are the frictional forces of the *VFPI* in the *x*- and *y*-directions, respectively; $k_b(z_b)$ is the instantaneous stiffness of the *VFPI*; z_b is the resultant isolator displacement; and x_b and y_b are the isolator displacement in *x*- and *y*-directions, respectively.

The instantaneous stiffness of the *VFPI* [20] can be written as

$$k_b(z_b) = M\,\omega_b^2(z_b) \tag{2}$$

$$\omega_b^2(z_b) = \left[\frac{\omega_i^2}{(1+r)^2\sqrt{(1+2r)}} \right] \tag{3}$$

$$r = \frac{z_b\,\mathrm{sgn}(z_b)}{d} \tag{4}$$

$$\omega_i^2 = \frac{gb}{d^2} \tag{5}$$

$$T_i = 2\pi\sqrt{\frac{d^2}{gb}} \tag{6}$$

where $M = \left(m_b + \sum_{i=1}^{N} m_i \right)$ is the total mass of the base-isolated building; m_b is the mass of base raft; m_i is the mass of the i^{th} superstructure floor; N is the total number of floors in the superstructure; g is the acceleration due to gravity; b and d are semi-minor axis and initial value of the semi-major axis (which is greater than zero) of sliding surface; and $\mathrm{sgn}(z_b)$ is incorporated to maintain the symmetry of the sliding surface about the central vertical axis. The signum function has a value of +1 for positive value of sliding displacement and -1 for negative value of sliding displacement; r is the non-dimensional parameter for the sliding surface; ω_b is the instantaneous frequency of the *VFPI* which depends on the geometry of the sliding surface; ω_i is the initial frequency of the *VFPI* at zero isolator displacement; and T_i is the initial time period of the *VFPI*.

It can be noticed that the ratio b/d^2 governs the initial frequency of the isolator. Similarly, the value of $1/d$ determines the rate of variation of isolator frequency, and this factor has been defined as frequency variation factor (*FVF*) [20]. It can also be seen from Eq. (5) that the rate of decrease of isolator frequency is directly proportional to the *FVF* for a given initial frequency.

The limiting value of the frictional force, F_s, to which the sliding system can be subjected in a particular direction is expressed as

$$F_s = \mu M g \tag{7}$$

where μ is the friction coefficient of the sliding system.

Thus, the modeling of the *VFPI* is required for the specific value of the two parameters, namely initial time period, T_i, and friction coefficient, μ.

3. Variable Friction Pendulum System

The *VFPS* [12-13] in regards of details and operation is similar to the *FPS*. The difference between the *FPS* and the *VFPS* is that the friction coefficient of the *FPS* is considered to be constant whereas the friction coefficient of the *VFPS* is varied in the form of a curve. Such variation of the friction coefficient in the *VFPS* can be achieved by gradually varying the roughness of spherical surface. The curve is chosen such that up to a certain value of displacement the frictional force increases and then it decreases with further displacement. This type of curve gives the isolator initial softness for smaller inputs, then provides stiffness for moderate inputs, and finally for large inputs it becomes soft again. The curve is selected with the criterion that the isolator displacement and the base shear under the selected near-fault ground motions decrease significantly without much alteration to superstructure acceleration. The equation adopted to define the curve for the friction coefficient, μ of the *VFPS* is as follows

$$\mu = (\mu_0 + a_1|z_b|)e^{-a_2|z_b|} \tag{8}$$

where μ_0 is the initial value of friction coefficient; a_1 and a_2 are the parameters that describe the variation of the friction coefficient along the sliding surface of the *VFPS*; $z_b = \sqrt{(x_b^2 + y_b^2)}$ is the resultant isolator displacement; and x_b and y_b are the displacement of the base mass relative to the ground in the *x*- and *y*-directions, respectively.

4. Modeling and Idealization of Building Isolated by the VFPI

Figure (2) shows the structural system under consideration which is an idealized *N*-story shear-type building resting on the *VFPI*. The *VFPI* is installed between the base mass and foundation of the building. The modeling of the *VFPI* is also shown in Figure (2). The various assumptions made for the system under consideration are as follows:

1. Superstructure is considered to be symmetric with respect to two orthogonal horizontal directions (i.e., there is no torsional coupling with lateral movement of the system), as a result, the system will have only the lateral degrees of freedom.
2. Floors of each story of superstructure are assumed as rigid.

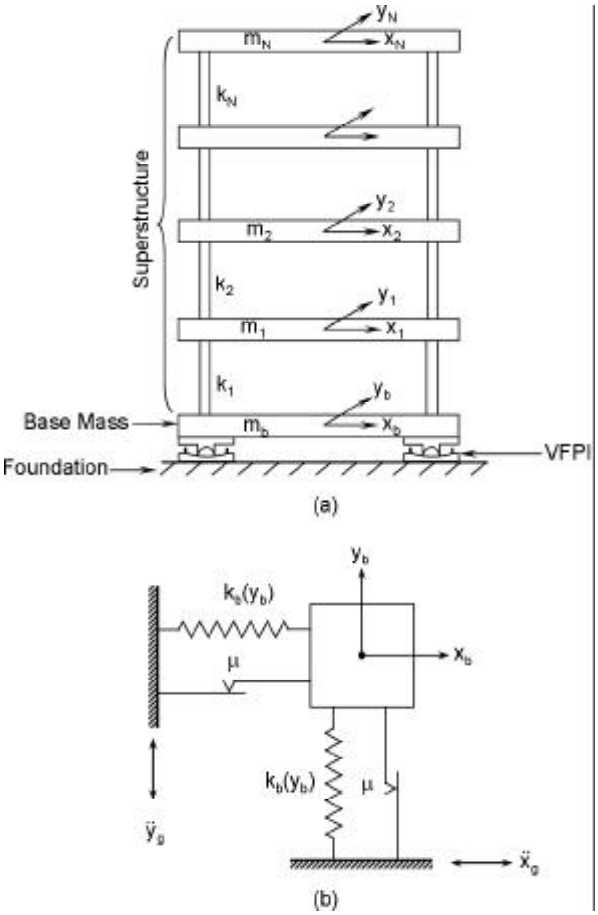

Figure 2. Modeling of multi-story building and the VFPI.

3. The force-deformation behaviour of the superstructure is considered to be linear with viscous damping.
4. Friction coefficient of the *VFPI* is assumed to be independent of the relative velocity at the sliding interface.
5. The *VFPI* is isotropic (i.e., there is same isolation period and the coefficient of friction in two orthogonal directions of the motion in the horizontal plane).
6. The slider of the isolator is assumed to have point contact with the sliding interface.
7. Restoring force provided by the *VFPI* is considered to be non-linear.
8. The frictional forces of the *VFPI* are assumed to be coupled in two directions.
9. No overturning or tilting takes place in the superstructure during sliding over the *VFPI*.
10. The fault normal and parallel components of near-fault ground motion are applied in two horizontal directions (referred as *x*- and *y*-directions, respectively) of the building isolated with the *VFPI*.

At each floor and base mass two lateral dynamic degrees of freedom are considered. Therefore, there are 2 x (N+1) dynamic degrees of freedom for the N-story superstructure. The equations governing the motion of an isolated N-story flexible shear-type building isolated with *VFPI* under the two horizontal components of earthquake excitation are expressed as

$$[M]\{\ddot{x}\}+[C]\{\dot{x}\}+[K]\{x\}=[M][r]\{\ddot{z}_g\} \tag{9a}$$

$$m_b\ddot{x}_b+F_{bx}-c_1\dot{x}_1-k_1x_1=-m_b\ddot{x}_g \tag{9b}$$

$$m_b\ddot{y}_b+F_{by}-c_1\dot{y}_1-k_1y_1=-m_b\ddot{y}_g \tag{9c}$$

where [M], [C] and [K] are the mass, damping and stiffness matrices of the superstructure, respectively, of the size $2N\times 2N$; $\{x\}=\{x_1,x_2,...,x_N,y_1,y_2,...,y_N\}^T$ is the displacement vector of the superstructure relative to the base mass; x_i and y_i is the lateral displacement of the i^{th} floor relative to the base mass in x- and y-directions, respectively; $\ddot{x}_b$ and $\ddot{y}_b$ are the acceleration of the base mass relative to the ground in the x- and y-directions, respectively; k_1 and c_1 are the stiffness and damping of the first story of the superstructure, respectively; [r] is the influence coefficient matrix; $\{\ddot{z}_g\}=(\ddot{x}_g+\ddot{x}_b,\ddot{y}_g+\ddot{y}_b)^T$ is the vector of base acceleration; $\ddot{x}_g$ and $\ddot{y}_g$ are the earthquake ground acceleration in the x- and y-directions; F_{bx} and F_{by} are the restoring forces of the *VFPI* in the x- and y-directions, respectively; T denotes the transpose; and over-dots indicate derivative with respect to time.

5. Criteria for Sliding and Non-Sliding Phases

In a non-sliding phase (i.e., $\ddot{x}_b=\ddot{y}_b=0$ and $\dot{x}_b=\dot{y}_b=0$), the resultant of the frictional forces mobilized at the interface of the *VFPI* is less than the limiting frictional force ($\sqrt{F_x^2+F_y^2}<F_s$) [21]. The system starts sliding (i.e., $\ddot{x}_b\neq\ddot{y}_b\neq 0$ and $\dot{x}_b\neq\dot{y}_b\neq 0$) as soon as the resultant of the frictional forces attains the limiting frictional force. Thus, the sliding of the system takes place if

$$\left(\frac{F_x}{F_s}\right)^2+\left(\frac{F_y}{F_s}\right)^2=1 \tag{10}$$

Note that Eq. (10) depicts the circular interaction between the frictional forces mobilized at the interface of the *VFPI*. The system remains in the non-sliding phase inside the interaction curve. It is to be noted that the equations of motion of the sliding structures in two orthogonal directions are coupled during the sliding phases due to interaction between the frictional forces. However, this interaction effect is ignored if the structural system is modeled as a 2-*D* system. In such cases, the corresponding curve which separates the sliding and non-sliding phases is a square as shown in Figure (3a) by dashed lines. Further, the system changes to non-sliding phase from the sliding phase whenever the resultant velocity of the base mass (i.e., $\dot{z}_b$) approaches zero.

Since the frictional forces oppose the motion of the system, the direction of the sliding of the system with respect to the x-direction is expressed as

$$\theta=\tan^{-1}\left(\frac{\dot{y}_b}{\dot{x}_b}\right) \tag{11}$$

where $\dot{x}_b$ and $\dot{y}_b$ are the velocities of the base mass relative to the ground in x- and y-directions, respectively.

6. Solution of Equations of Motion

The frictional forces mobilized in the *VFPI* are non-linear functions of the displacement and velocity of the system in two orthogonal directions. Also, during the sliding phase of motion, the mobilized frictional forces are coupled with each other by the circular interaction (see Eq. (10)). As a result, the equations of motion are solved in the incremental form by employing the Newmark-β method assuming linear variation of acceleration over the small time interval, Δt. The incremental equations in terms of unknown incremental displacements are expressed as

$$\left[K_{eff}\right]\{Dx\}=\left\{P_{eff}\right\}+\{Df\} \tag{12}$$

where K_{eff} is the effective stiffness matrix; $\{Dx\}$ is the incremental displacement vector; $\{P_{eff}\}$ is the effective excitation vector; and $\{Df\}$ is the incremental frictional force vector.

With a view to determine the incremental frictional forces, consider Figure (3b). At time t the frictional forces are at point A on the interaction curve and move to point B at time $t+\Delta t$. Therefore, the incremental frictional forces in the x- and y-directions, respectively, are expressed as:

$$Df_x=F_s\cos(\theta^{t+Dt})-F_x^t \tag{13a}$$

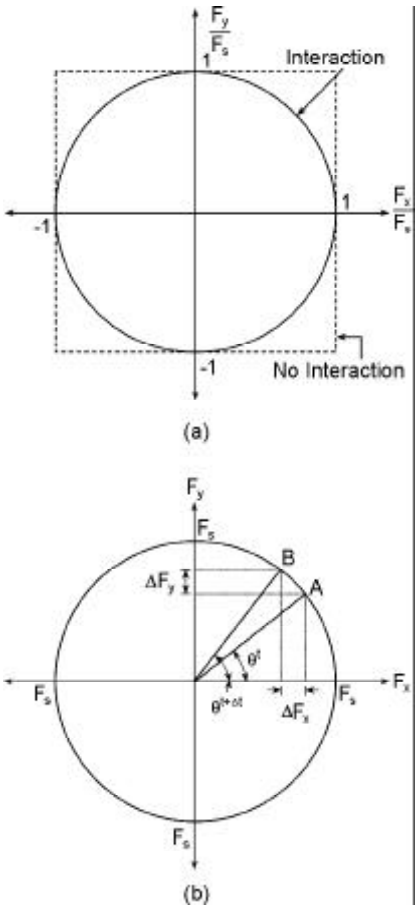

Figure 3. Interaction and incremental frictional forces in two orthogonal directions of the VFPI.

$$Df_y = F_s \sin(\theta^{t+Dt}) - F_y^t \tag{13b}$$

where the superscript denotes the time.

Since the frictional forces are opposite to the motion of the system, therefore, the angle θ^{t+Dt} is expressed in terms of the relative velocities of the system at time $t+Dt$ by

$$\theta^{t+Dt} = \tan^{-1}\left(\frac{\dot{y}_b^{t+Dt}}{\dot{x}_b^{t+Dt}}\right) \tag{14}$$

Substituting for θ^{t+Dt} in Eq. (14), the incremental frictional forces are expressed as

$$DF_x = F_s \frac{\dot{x}_b^{t+Dt}}{\sqrt{\left(\dot{x}_b^{t+Dt}\right)^2 + \left(\dot{y}_b^{t+Dt}\right)^2}} - F_x^t \tag{15a}$$

$$DF_y = F_s \frac{\dot{y}_b^{t+Dt}}{\sqrt{\left(\dot{x}_b^{t+Dt}\right)^2 + \left(\dot{y}_b^{t+Dt}\right)^2}} - F_y^t \tag{15b}$$

In order to solve the incremental matrix Eq. (12), the incremental frictional forces (Df_x and Df_y) should be known at any time interval. The incremental frictional forces involve the system velocities at time $t+Dt$ (see Eq. (15)) which in turn depend on the incremental displacements (Dx_b and Dy_b) at the current time step. As a result, an iterative procedure is required to obtain the required incremental solution. The steps of the procedure considered are as follows:

1. Assume $DF_x = DF_y = 0$ for iteration, j = 1 in Eq. (12) and solve for Dx_b and Dy_b.
2. Calculate the incremental velocity $D\dot{x}_b$ and $D\dot{y}_b$ using the Dx_b and Dy_b.
3. Calculate the velocities at time $t+Dt$ using incremental velocities (i.e., $\dot{x}_b^{t+Dt} = \dot{x}_b^t + D\dot{x}_b$ and $\dot{y}_b^{t+Dt} = \dot{y}_b^t + D\dot{y}_b$) and compute the revised incremental frictional forces DF_x and DF_y from Eq. (15).
4. Iterate further, until the following convergence criteria are satisfied for both incremental frictional forces, i.e.,

$$\frac{\left|\left(DF_x\right)^{j+1}\right| - \left|\left(DF_x\right)^{j}\right|}{\left|\left(DF_x\right)^{j}\right|} \le \varepsilon \tag{16a}$$

$$\frac{\left|\left(DF_y\right)^{j+1}\right| - \left|\left(DF_y\right)^{j}\right|}{\left|\left(DF_y\right)^{j}\right|} \le \varepsilon \tag{16b}$$

where ε is a small threshold parameter. The superscript to the incremental forces denotes the iteration number.

When the convergence criteria are satisfied, the velocity of the sliding structure at time $t+Dt$ is calculated using incremental velocity. In order to avoid the unbalance forces, the acceleration of the system at time $t+Dt$ is evaluated directly from the equilibrium of system Eq. (9). The response of the sliding structures is quite sensitive to the time interval, Dt, and initial conditions at the beginning of sliding and non-sliding phases. For the present study, the results are obtained with maximum time interval, Dt = 0.0001*sec*. In order to determine the incremental frictional forces at the sliding support, the number of iterations in each time step is taken as 10. At the end of each time step the phase of the motion of the system should be checked. Further, the sliding velocity less than 1×10-8*m/sec* is assumed to be zero for checking the transition from sliding to non-sliding phase.

7. Numerical Study

For the present study, the mass matrix of the superstructure, [*M*], is diagonal and characterized by the mass of each floor which is kept constant (i.e., $m_i = m$ for $i = 1$ to N). Also, for simplicity the stiffness of all the floors is taken as constant and expressed by the parameter *k*. The value of *k* is selected to provide the required fundamental time period of superstructure, T_s, as a fixed base. The damping matrix of the superstructure, [*C*], is not known explicitly. It is constructed by assuming the modal damping ratio which is kept constant in each mode of vibration. Thus, the superstructure and the base mass of the isolated structural system under consideration can be completely characterized by the parameters namely, the fundamental time period of the superstructure, T_s, damping ratio of the superstructure, x_s, number of stories in the superstructure, *N*, and the ratio of base mass to the superstructure floor mass, m_b/m. The superstructure considered has five stories with fundamental time period, T_s = 0.5*sec* and damping ratio, x_s = 2% of critical damping. The fundamental time period and damping ratio of the superstructure are considered to be equal in the *x*- and *y*-directions. The mass ratio, m_b/m, is assumed to be unity. On the other hand, the *VFPI* isolator is characterized by two parameters, namely initial time period, T_i, and the coefficient of friction, μ. For all investigations, the parameters of the *VFPI* are selected as $b = 0.01m$ and $d = 0.1m$ (*FVF* 10 per *m*) so that it has initial time period of 2.0*sec*. The value of μ has been considered as 0.02. For comparison, examples with the *FPS* and *VFPS* isolators are also taken with isolation period of 2.0*sec*. The *VFPS* isolators are characterized by two parameters, namely the period of the base isolation, T_b, and the coefficient of friction, μ. The coefficient of sliding friction, μ, in the *VFPS* can be defined by the initial time period of the *VFPS*, T_i, and the peak frictional coefficient, μ_{max}. In case of the *VFPS* isolator, an initial time period of 1.5*sec* and a peak friction coefficient of 0.15 are chosen for all investigations. In case of the *FPS* isolators, a coefficient of sliding friction of 0.02 is selected for all investigations. In the present study, the superstructure parameters, x_s and m_b/m, are held constant.

The response quantities of interest are the top floor absolute acceleration (i.e., $\ddot{x}_a = \ddot{x}_N + \ddot{x}_b + \ddot{x}_g$ and $\ddot{y}_a = \ddot{y}_N + \ddot{y}_b + \ddot{y}_g$), the base shear (i.e., F_{bx} and F_{by}) and the isolator displacement (i.e., x_b and y_b) in the *x*- and *y*-directions. The top floor absolute acceleration and base shear are directly proportional to the forces (shear force and bending moments) exerted in the superstructure due to the earthquake ground motion. On the other hand, the relative displacements of the *VFPI* are crucial from the design point of view of the isolator.

Six pairs of near-fault ground motions are used as input ground motions in order to effectively study the dynamic behaviour of building isolated with the *VFPI* under bi-directional excitation. Some characteristics of these recorded near-fault ground motions are summarized in Table (1). From this table, it is found that these near-fault ground motions have a variety of *PGA*, *PGV* and *PGD*. It is observed that in most of the cases, the *PGA* of fault normal component is relatively higher than that of fault parallel component. Furthermore, the acceleration and displacement spectra of the six ground motions for 5% damping are shown in Figure (4). The spectra of these ground motions indicate that the ground motions are recorded at a firm soil or rock site. From this figure, it is found that the average spectral acceleration and displacement

Table 1. Some characteristics of near-fault ground motions considered in the study.

Near-Fault Ground Motions	Recording Station	Duration (sec)	Normal Component			Parallel Component		
			PGD (cm)	PGV (cm/sec)	PGA (g)	PGD (cm)	PGV (cm/sec)	PGA (g)
January 17, 1994 Northridge, California	Sylmar	60.000	31.1	122	0.73	9.03	53.9	0.6
January 17, 1994 Northridge, California	Rinaldi	14.950	39.1	175	0.89	18.4	60.2	0.39
January 17, 1994 Northridge, California	Newhall	60.000	38.1	119	0.72	17.6	49.3	0.65
June 28, 1992 Landers, California	Lucerne Valley	49.284	230	136	0.71	184	70.3	0.80
October 15, 1979 Imperial Valley, California	El Centro Array #5	39.420	76.5	98	0.37	150	52.5	0.55
October 15, 1979 Imperial Valley, California	El Centro Array #7	36.900	49.1	113	0.46	218	55.2	0.34

Note: PGD = Peak Ground Displacement, PGV= Peak Ground Velocity and PGA= Peak Ground Acceleration

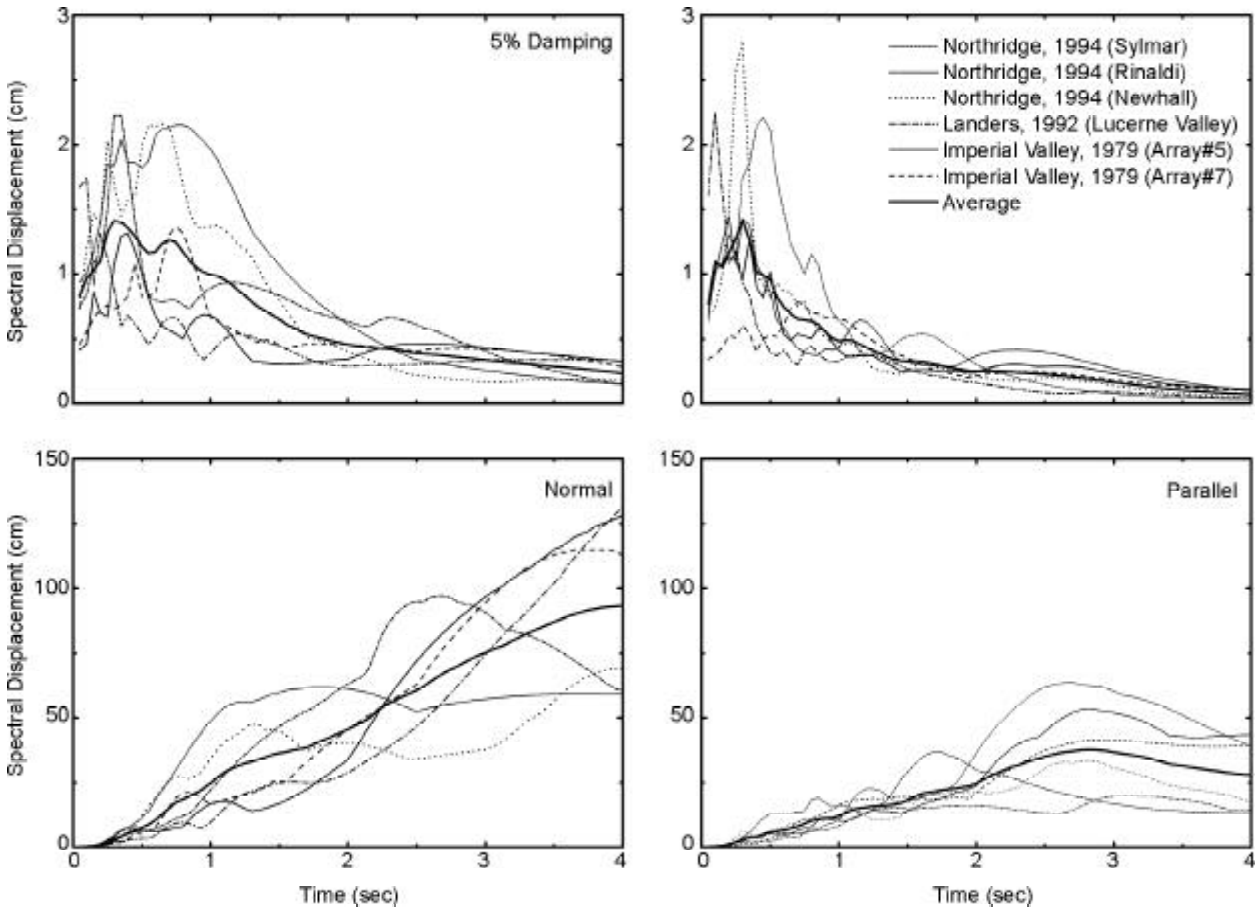

Figure 4. Acceleration and displacement spectra of the six near-fault ground motions for 5% damping.

values of the fault normal and parallel component is almost the same for low periods (i.e., in the range 0-0.3*sec*). For longer periods (i.e., beyond 0.3*sec*), the spectral acceleration and displacement component of fault normal component is significantly larger than the fault parallel component.

7.1. Comparison of the Isolators Considering Interaction of the Friction Forces

Table (2) shows the comparison of the peak response quantities of the three isolators considering the interaction of the friction forces. This table shows that in most of the near-fault ground motions, the responses, especially top floor absolute acceleration and base shear of structures with the *VFPI* are considerably reduced as compared to those structures with the *FPS* and *VFPS* isolators, whereas the isolator displacement of the *VFPI* exceeds that of the *FPS* and the *VFPS*. This is expected as the horizontal stiffness of the *VFPI* is lower than that of the *FPS* and the *VFPS*. Such large isolator displacement of the *VFPI* will lead to the requirement of very large isolators, costly flexible connections for utilities and an extensive and expensive loss of space for a seismic gap. Under near-fault ground motions, this feature of the *VFPI* reduces its effectiveness in comparison to the *FPS* and the *VFPS*. In order to give further insight into the difference in the behavior of structures with the *VFPI*, *FPS* and *VFPS* isolators, time histories of top floor absolute acceleration and isolator displacement are shown in Figure (5) for Northridge, 1994 (Sylmar) and Northridge, 1994 (Rinaldi) near-fault ground motions. Similar trends observed in Figure (5) and Table (2), are also observed in Figure (6) which shows the comparison of the hysteresis loops of the *VFPI*, *FPS* and *VFPS* isolators.

7.2. Comparison between Isolator Displacement in the x- and y-Directions

Figure (7) shows the time variation of x_b and y_b of the building isolated with the *VFPI* (T_i = 2.0*sec* and μ = 0.02) under different near-fault ground motions (top); and correlation between x_b and y_b (bottom). The peak values of x_b and y_b for Northridge, 1994 (Sylmar) near-fault ground motion are 63.588

Table 2. Comparison between peak response quantities of various isolators considering the interaction of the friction forces.

Near-fault Ground Motions	Building Condition	$\ddot{x}_a$ (g)	$\ddot{y}_a$ (g)	F_{bx}(W)	F_{by} (W)	x_b (cm)	y_b (cm)
Northridge, 1994 (Sylmar)	Isolated (FPS)	0.8564	0.4024	0.7293	0.3198	71.9780	31.7210
	Isolated (VFPI)	0.1604	0.1410	0.0342	0.0303	63.5880	16.8440
	Isolated (VFPS)	0.8008	0.4739	0.4126	0.2542	40.0610	22.4930
Northridge, 1994 (Rinaldi)	Isolated (FPS)	0.8493	0.5163	0.7525	0.4470	72.9400	43.8890
	Isolated (VFPI)	0.2037	0.1825	0.0340	0.0303	63.6420	40.4250
	Isolated (VFPS)	0.8165	0.5370	0.5101	0.2508	50.0200	22.0930
Northridge, 1994 (Newhall)	Isolated (FPS)	0.5275	0.3107	0.4382	0.2255	42.8360	22.3720
	Isolated (VFPI)	0.2426	0.1895	0.0339	0.0266	82.9760	44.8440
	Isolated (VFPS)	1.0045	0.6904	0.2768	0.1994	18.6420	9.8999
Landers, 1992 (Lucerne Valley)	Isolated (FPS)	0.4260	0.3086	0.3168	0.1546	30.9040	13.9400
	Isolated (VFPI)	0.2324	0.3075	0.0354	0.0346	120.3700	72.9390
	Isolated (VFPS)	0.7048	0.7898	0.2897	0.1630	21.5940	10.3140
Imperial Valley, 1979 (El Centro Array #5)	Isolated (FPS)	0.5691	0.3096	0.4782	0.2311	47.3160	22.6330
	Isolated (VFPI)	0.1519	0.1973	0.0287	0.0287	123.9000	102.8500
	Isolated (VFPS)	0.7407	0.4165	0.2800	0.1867	23.4070	6.7835
Imperial Valley, 1979 (El Centro Array #7)	Isolated (FPS)	0.4277	0.2927	0.3831	0.2426	37.7590	24.0500
	Isolated (VFPI)	0.1239	0.1010	0.0355	0.0252	113.4200	74.9270
	Isolated (VFPS)	0.7162	0.8309	0.2793	0.2053	17.5720	9.9297

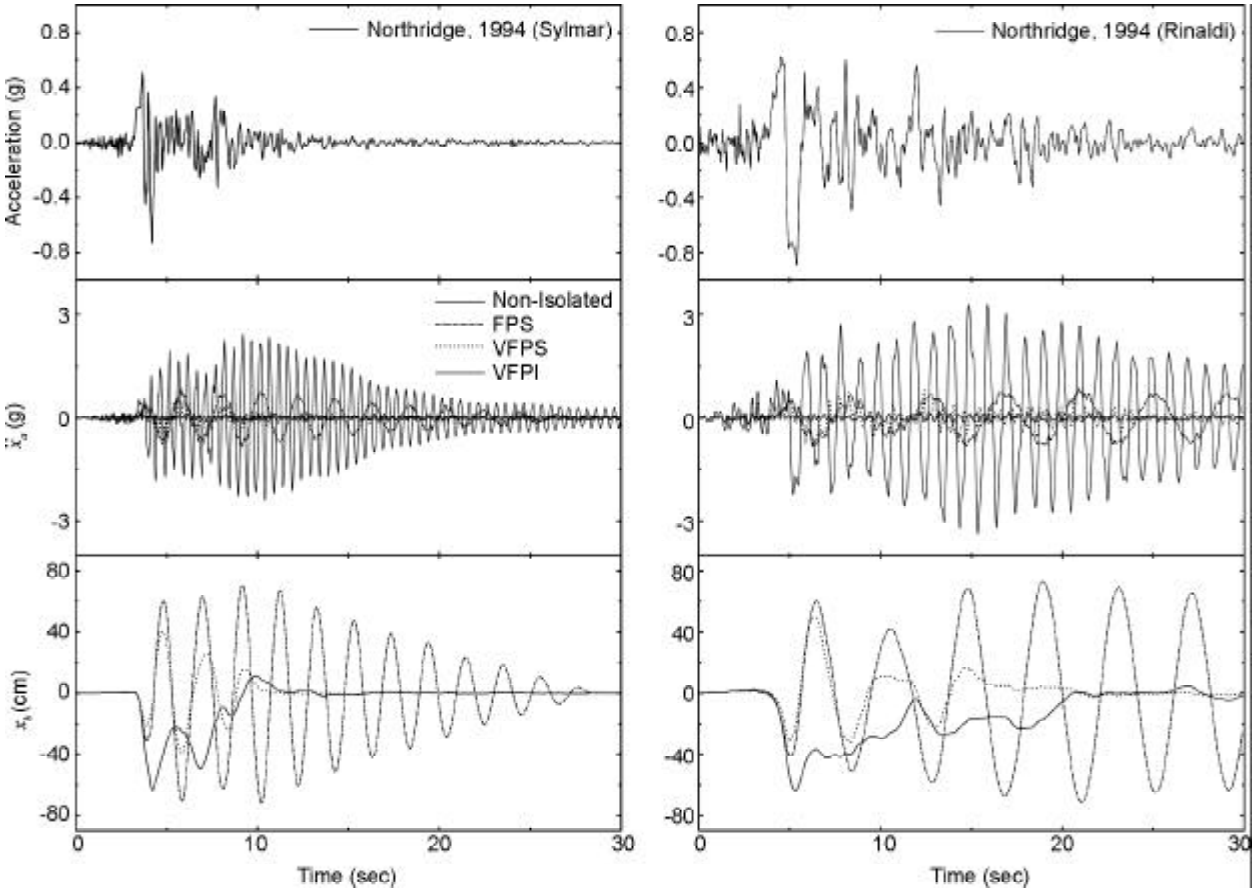

Figure 5. Time variation of top floor absolute acceleration and isolator displacement of five-story building isolated with the FPS (T_b = 2.0sec and μ = 0.02), VFPS (T_b = 2.0sec, T_i = 1.5 sec and μ_{max} = 0.15) and VFPI (T_i = 2.0 sec and μ = 0.02) under Northridge, 1994 (Sylmar) and Northridge, 1994 (Rinaldi) near-fault ground motions.

and 16.844*cm*, respectively whereas for Northridge, 1994 (Rinaldi) near-fault ground motion are 63.642 and 40.425*cm*, respectively. From this figure, it can be noticed that the peak isolator displacement in fault normal direction, x_b, is significantly larger than the corresponding peak isolator displacement in fault parallel direction, y_b. This is expected due to the fact that spectral content of fault normal component

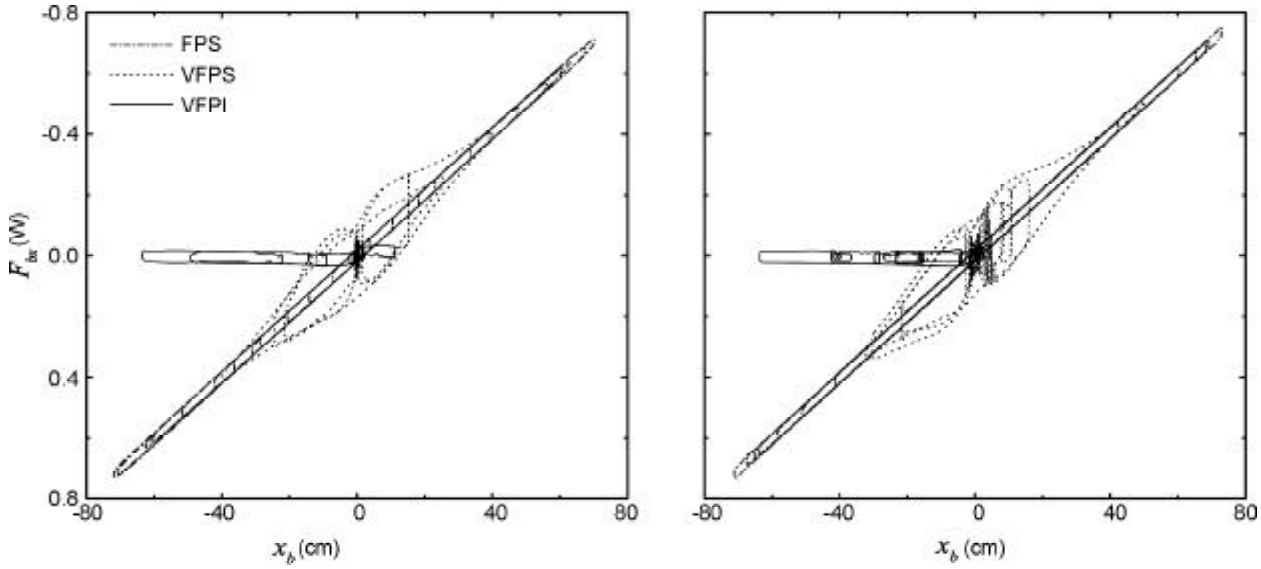

Figure 6. Comparison between hysteresis loops of the FPS, VFPS and VFPI isolators.

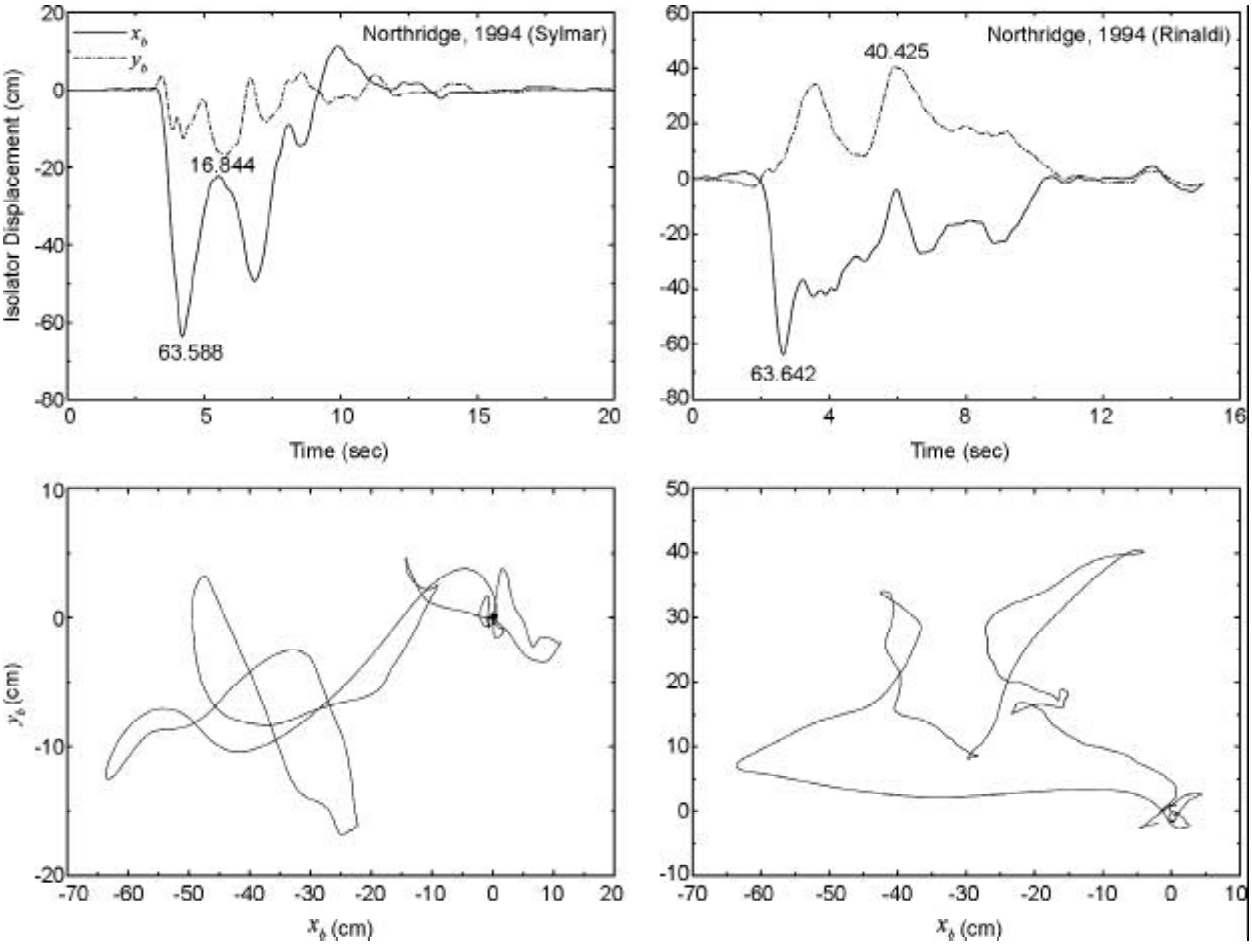

Figure 7. Top: Time variation of x_b and y_b of five-story building isolated with VFPI (T_i = 2.0sec and μ = 0.02) under different near-fault ground motions. Bottom: Correlation between x_b and y_b.

is considerably larger than the fault parallel component of near-fault ground motion. Furthermore, it is observed that the response of isolated systems to fault normal and fault parallel components are more or less uncorrelated as the maximum displacement in the fault normal direction occurs at a different time than that in the fault parallel direction.

Figure (8) shows variation of peak displacements, x_b, y_b, z_b and z_m of the five-story building isolated with the *VFPI* against *FVF* for different types of near-fault ground motions. The displacement, z_m, denotes the square root of the sum of the squares (*SRSS*) of the peak values of x_b and y_b. As noted earlier, the displacement due to parallel component, y_b, is much smaller in comparison to the corresponding displacement due to the normal component, x_b. Furthermore, there is no significant difference between the peak resultant displacement, z_b, and the corresponding displacement, x_b, implying that the peak resultant displacement of the isolators is mainly contributed by the displacement due to the normal component of the near-fault ground motions. The displacement, z_m, is larger than displacement, z_b, confirming that the peak displacements in the isolation system due to the normal and parallel components of the near-fault motions do not occur at the same time. Similar trends can be also observed from Table (3).

7.3. Influence of Bi-Directional Interaction of the Friction Forces

The time variation of the absolute acceleration of superstructure (i.e., $\ddot{x}_a$ and $\ddot{y}_a$) and the sliding base displacement (i.e., x_b and y_b) in *x*- and *y*-directions are shown in Figure (9) for Northridge, 1994 (Sylmar) near-fault ground motion. The response is plotted for both considering and ignoring the interaction of the frictional forces of the *VFPI*. The absolute acceleration of the superstructure is relatively less for considering the effects of the interaction of frictional forces as compared to those without interaction. Thus, the superstructure experiences

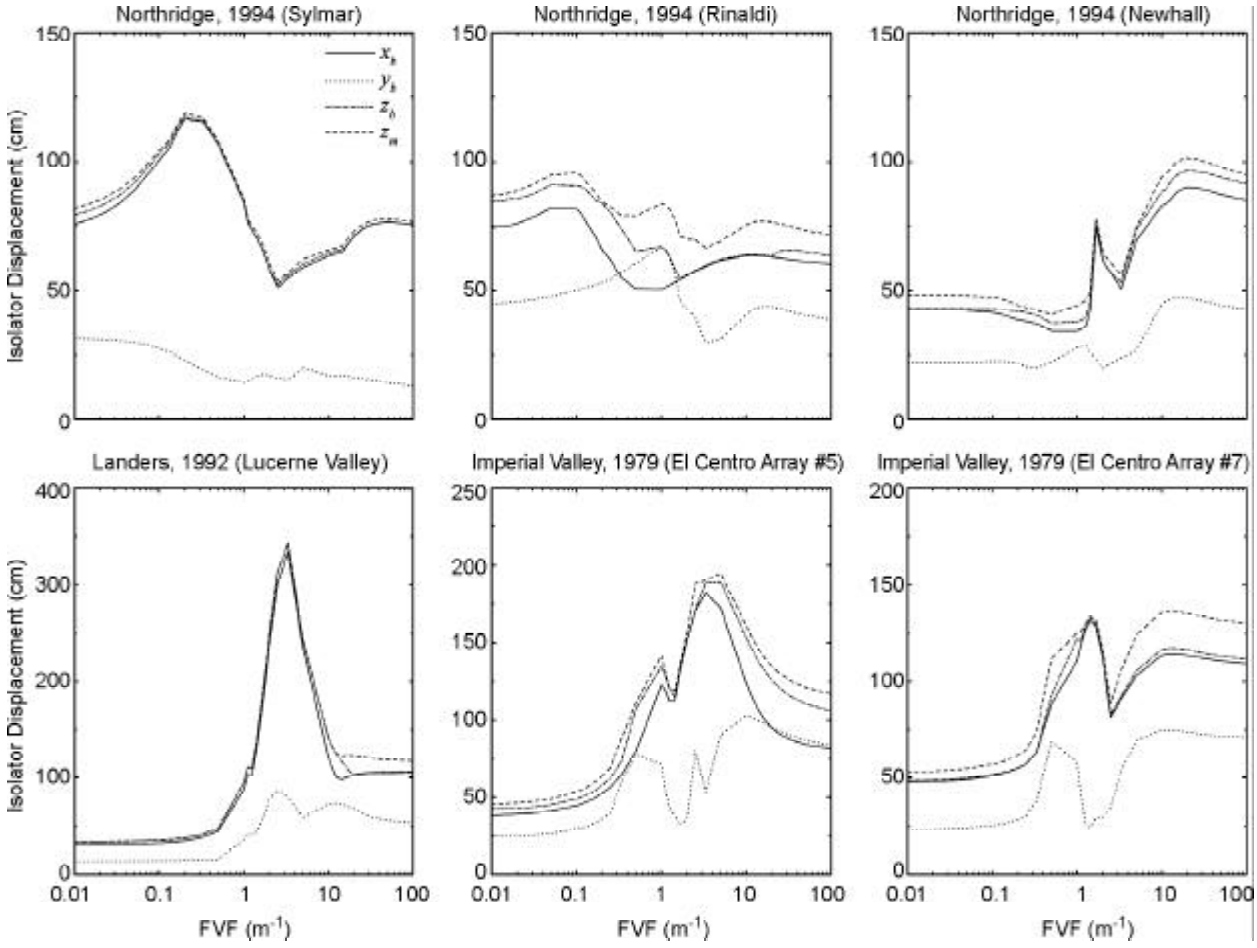

Figure 8. Variation of the peak isolator displacements, x_b, y_b, z_b, and z_m, of five-story building isolated with the VFPI against the FVF for various near-fault ground motions.

Table 3. Peak response quantities of non-isolated building and VFPI-isolated building (T_i = 2sec and μ = 0.02).

Near-Fault Ground Motions	Building Condition	$\ddot{x}_a$ (g)	$\ddot{y}_a$ (g)	F_{bx} (W)	F_{by} (W)	x_b (cm)	y_b (cm)	z_b (cm)	z_m (cm)
Northridge, 1994 (Sylmar)	Non-isolated	2.4362	4.1222	1.4504	2.5888	---	---	---	---
	Isolated (No interaction)	0.2477	0.2975	0.0359	0.0359	62.1700	15.4140	64.0523	64.0523
	Isolated (Interaction)	0.1604	0.1410	0.0342	0.0303	63.5880	16.8440	64.7450	65.7810
Northridge, 1994 (Rinaldi)	Non-isolated	3.3692	2.2774	1.9843	1.2256	---	---	---	---
	Isolated (No interaction)	0.4108	0.3075	0.0359	0.0359	62.5110	27.9180	68.4620	68.4620
	Isolated (Interaction)	0.2037	0.1825	0.0340	0.0303	63.6420	40.4250	64.0360	75.3950
Northridge, 1994 (Newhall)	Non-isolated	4.3521	1.5202	2.5312	0.6983	---	---	---	---
	Isolated (No interaction)	0.2835	0.3250	0.0359	0.0359	81.1890	19.4310	83.4818	83.4818
	Isolated (Interaction)	0.2426	0.1895	0.0339	0.0266	82.9760	44.8440	88.4580	94.3190
Landers, 1992 (Lucerne Valley)	Non-isolated	2.3189	1.9496	0.6026	0.5309	---	---	---	---
	Isolated (No interaction)	0.2993	0.4386	0.0359	0.0359	125.3900	13.9530	126.1639	126.1639
	Isolated (Interaction)	0.2324	0.3075	0.0354	0.0346	120.3700	72.9390	140.7300	140.7500
Imperial Valley, 1979 (El Centro Array #5)	Non-isolated	1.6985	2.8422	1.0542	1.3206	---	---	---	---
	Isolated (No interaction)	0.2565	0.2615	0.0359	0.0359	147.9800	77.4810	167.0371	167.0371
	Isolated (Interaction)	0.1519	0.1973	0.0287	0.0287	123.9000	102.8500	153.3800	161.0300
Imperial Valley, 1979 (El Centro Array #7)	Non-isolated	1.3789	0.9177	0.7753	0.5546	---	---	---	---
	Isolated (No interaction)	0.1578	0.2568	0.0359	0.0359	111.7700	22.6620	114.0443	114.0443
	Isolated (Interaction)	0.1239	0.1010	0.0355	0.0252	113.4200	74.9270	116.5300	135.9300

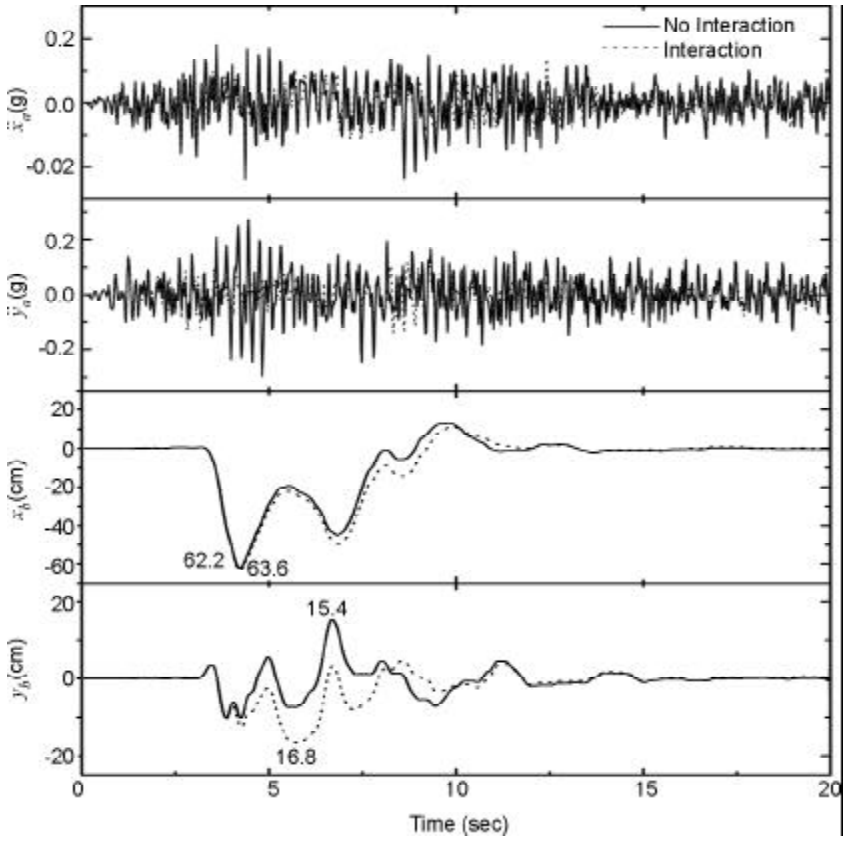

Figure 9. Time history of the absolute acceleration of the superstructure and isolator displacement to the Northridge, 1994 (Sylmar) near-fault ground motion.

less earthquake forces when the interaction of the frictional forces is considered in the analysis. On the other hand, the isolator displacements are relatively more for considering the interaction effects in comparison to that without interaction effects. This is due to the fact that when the interaction is taken into consideration the structure starts sliding at a relatively lower value of the frictional forces mobilized at the sliding interface (refer to the sliding Eq. (10)), and as a result, there is more isolator displacement. Similar trends in the response of the building isolated with the *VFPI* are found in Figure (10) for Northridge, 1994 (Rinaldi) near-fault ground motion. This implies that there is significant over prediction of the superstructure accelerations and under prediction of the isolator displacements under near-fault ground motions, if the bi-directional interaction effects are ignored and the system is idealized as a 2-*D* system. The under prediction of the isolator displacement is crucial from the point of view of designing the friction base isolators. Therefore, the bi-directional interaction effects of frictional forces of *VFPI* under near-fault ground motions must be rigorously considered in the analysis of the structure.

Figure (11) shows the variation of the resultant peak absolute acceleration of the superstructure (i.e., $\sqrt{(\ddot{x}_a)^2_{max}+(\ddot{y}_a)^2_{max}}$) against T_s under different near-fault ground motions. The figure indicates that for all values of superstructure time periods, the absolute acceleration of the superstructure is less for considering the interaction as compared to those without interaction. The absolute acceleration spectra of the superstructure without sliding support (referred to as non-isolated) are also shown in order to study the effectiveness of the sliding support. The figure indicates clearly that the sliding support is quite effective in reducing the earthquake response of the superstructure. Further, the absolute acceleration of the system with sliding base is less sensitive to the time period of the superstructure in comparison with fixed base system. Similar differences are also found in Figures (12) and (13) and Table (3).

In Figure (14), the variation of the resultant peak sliding base displacement is plotted against μ for various near-fault ground motions. The figure clearly shows that the peak isolator displacement is significantly higher for considering the interaction as

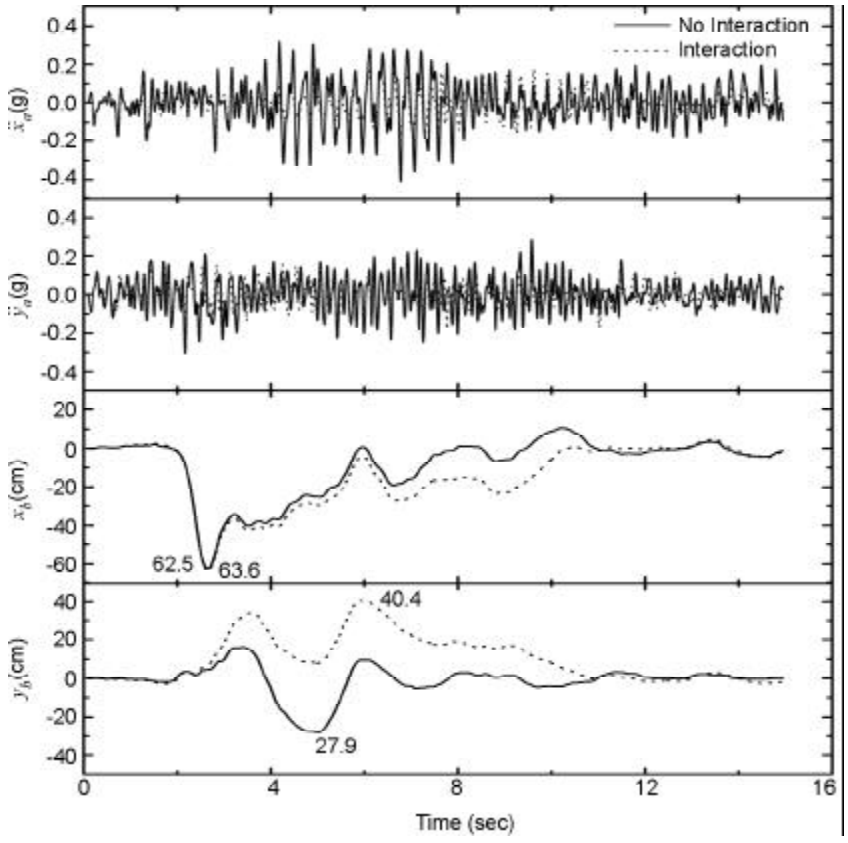

Figure 10. Time history of the absolute acceleration of the superstructure and isolator displacement to the Northridge, 1994 (Rinaldi) near-fault ground motion.

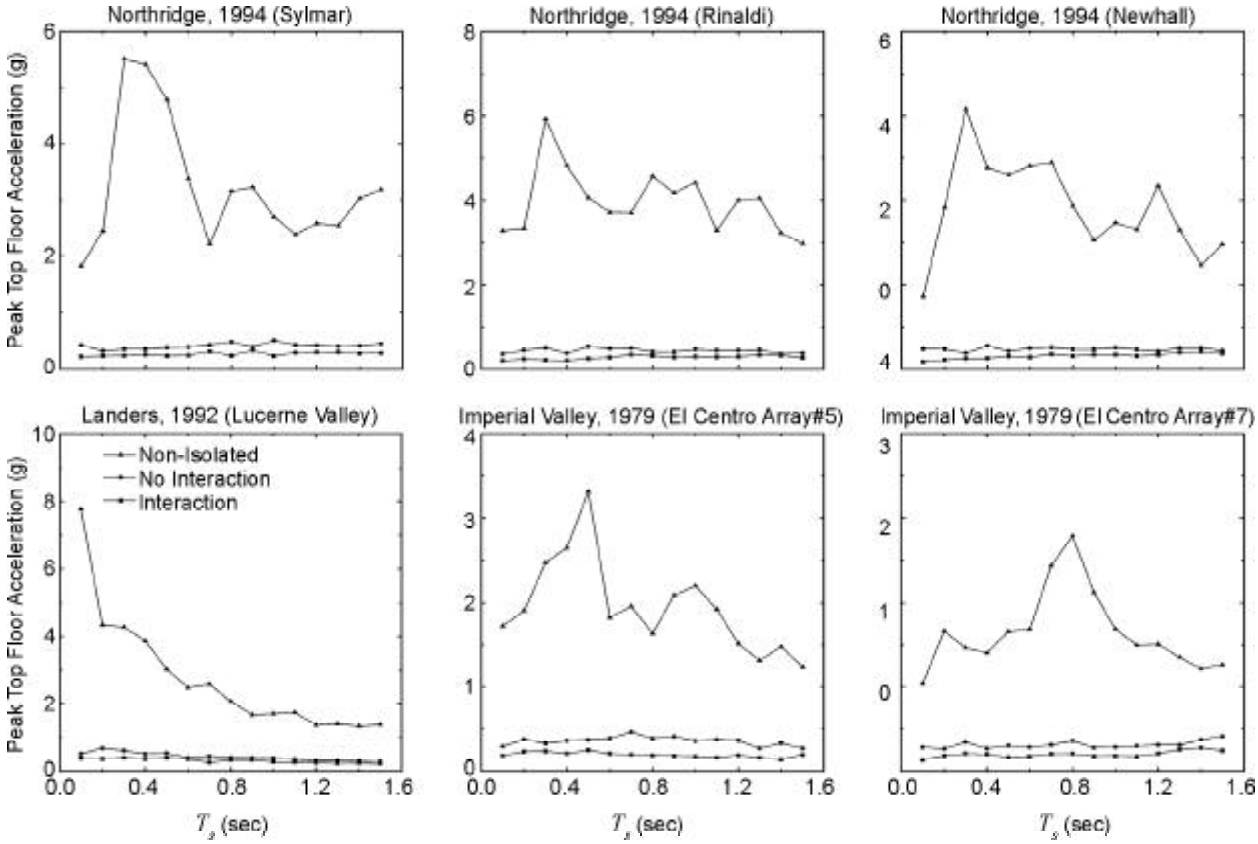

Figure 11. Effects of bi-directional interaction of frictional forces on peak absolute acceleration of the superstructure of five-story building isolated with the VFPI (T_i = 2.0 sec and μ = 0.02) under various near-fault ground motions.

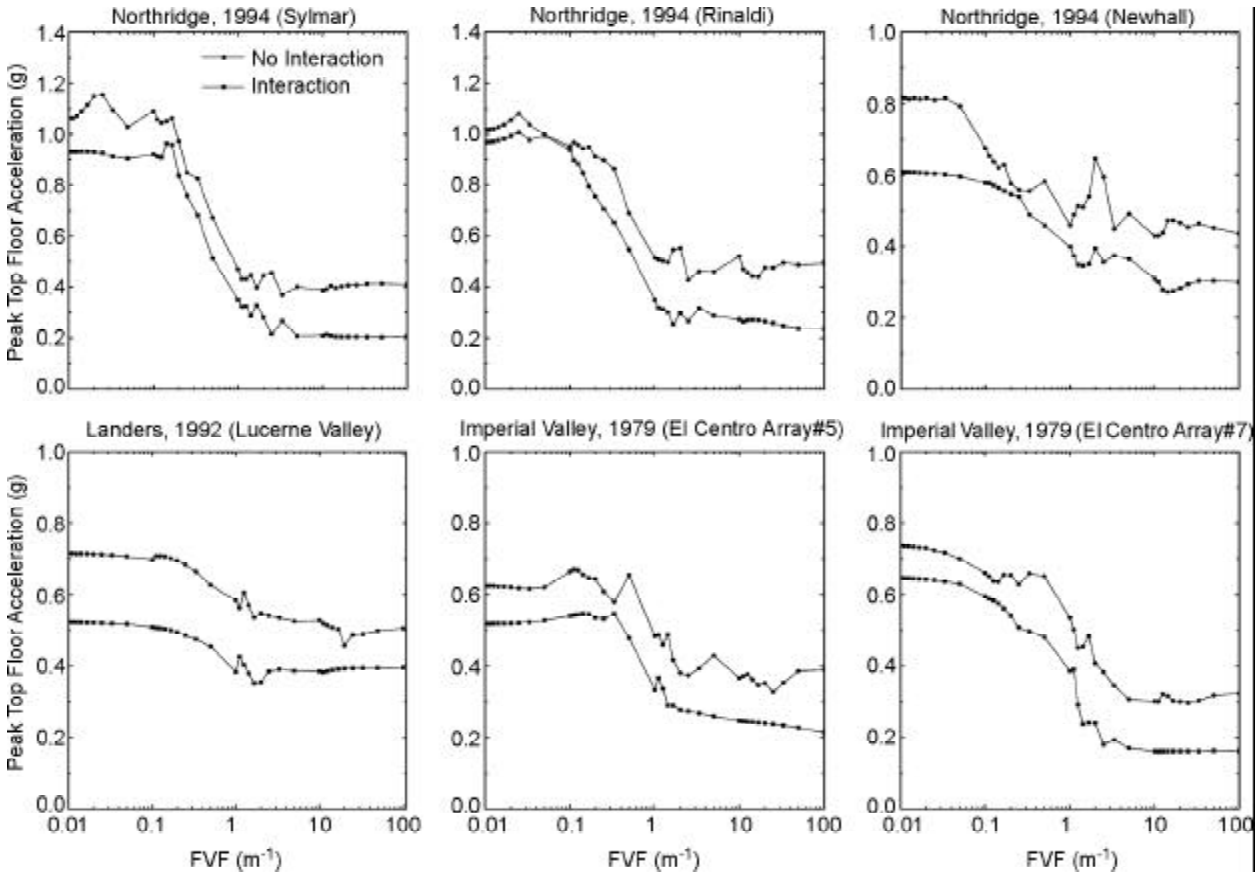

Figure 12. Plot of peak absolute superstructure acceleration of five-story building isolated with the VFPI against the FVF for various near-fault ground motions (considering with and without interaction).

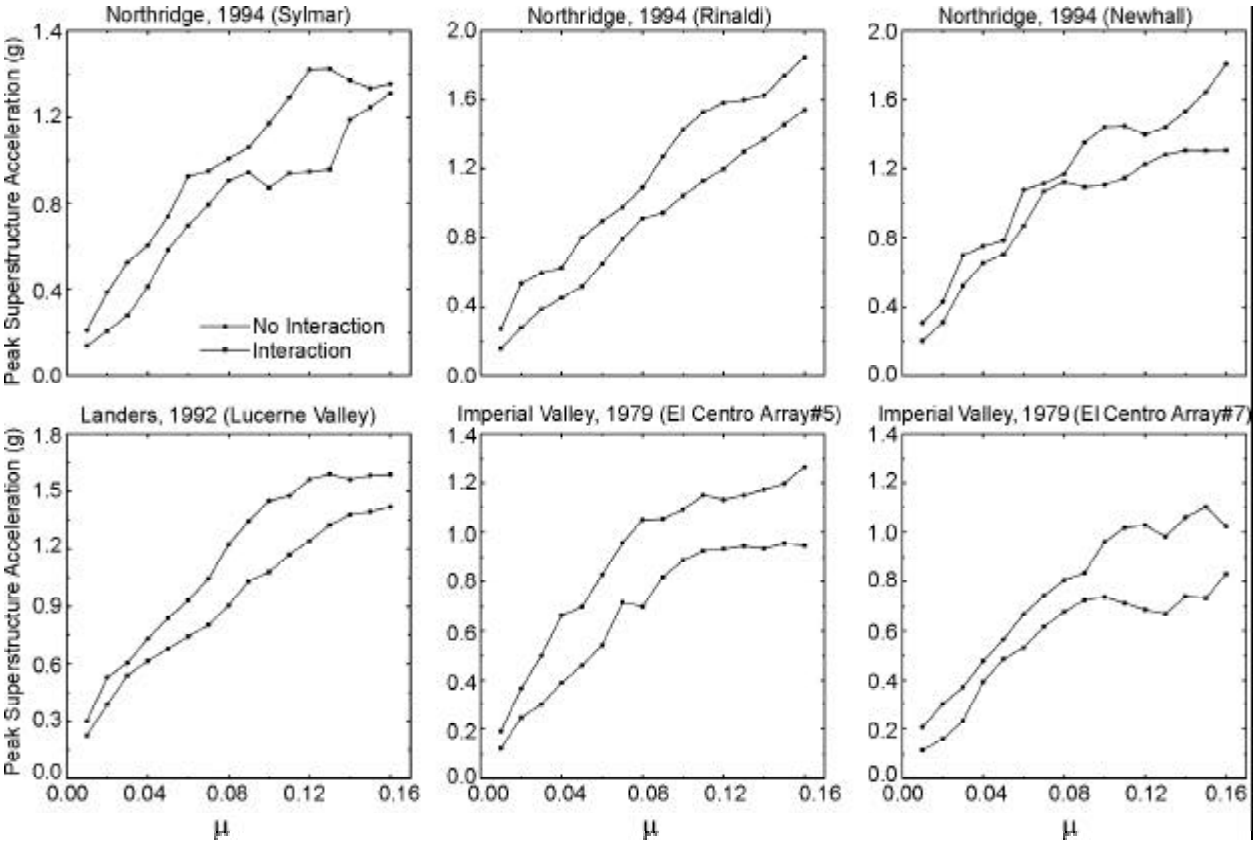

Figure 13. Friction coefficient variation of peak absolute superstructure acceleration of five-story building isolated with the VFPI under various near-fault ground motions (considering with and without interaction).

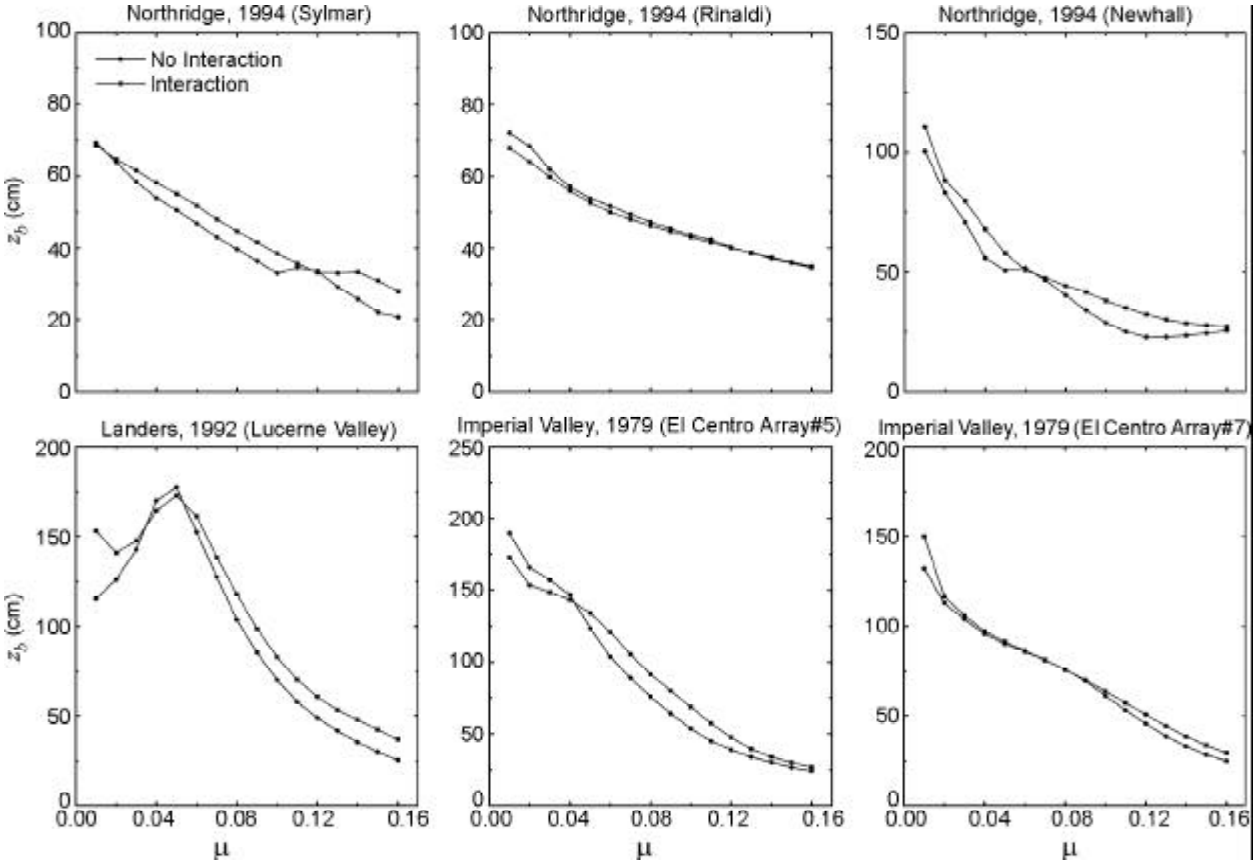

Figure 14. Comparison of isolator displacement of five-story building isolated by the VFPI during various near-fault ground motions (considering with and without interaction).

compared to those without interaction. Similar differences are also observed in Figure (15). Thus, there is a need to consider the bi-directional interaction effects of frictional forces on the response. Note that similar effects of bi-directional interaction of frictional forces for structures isolated by Teflon sliding bearing were observed by Mokha et al [22] and the same are further confirmed in the present study for *VFPI*-isolated structures.

In Figure (16), the variation of ratios, R_1 and R_2, is plotted against the friction coefficient of *VFPI* for various near-fault ground motions. The ratio, R_1, denotes the ratio of peak resultant isolator displacement with interaction to the corresponding displacement without interaction of frictional forces. The ratio, R_1, is an index of the bi-directional

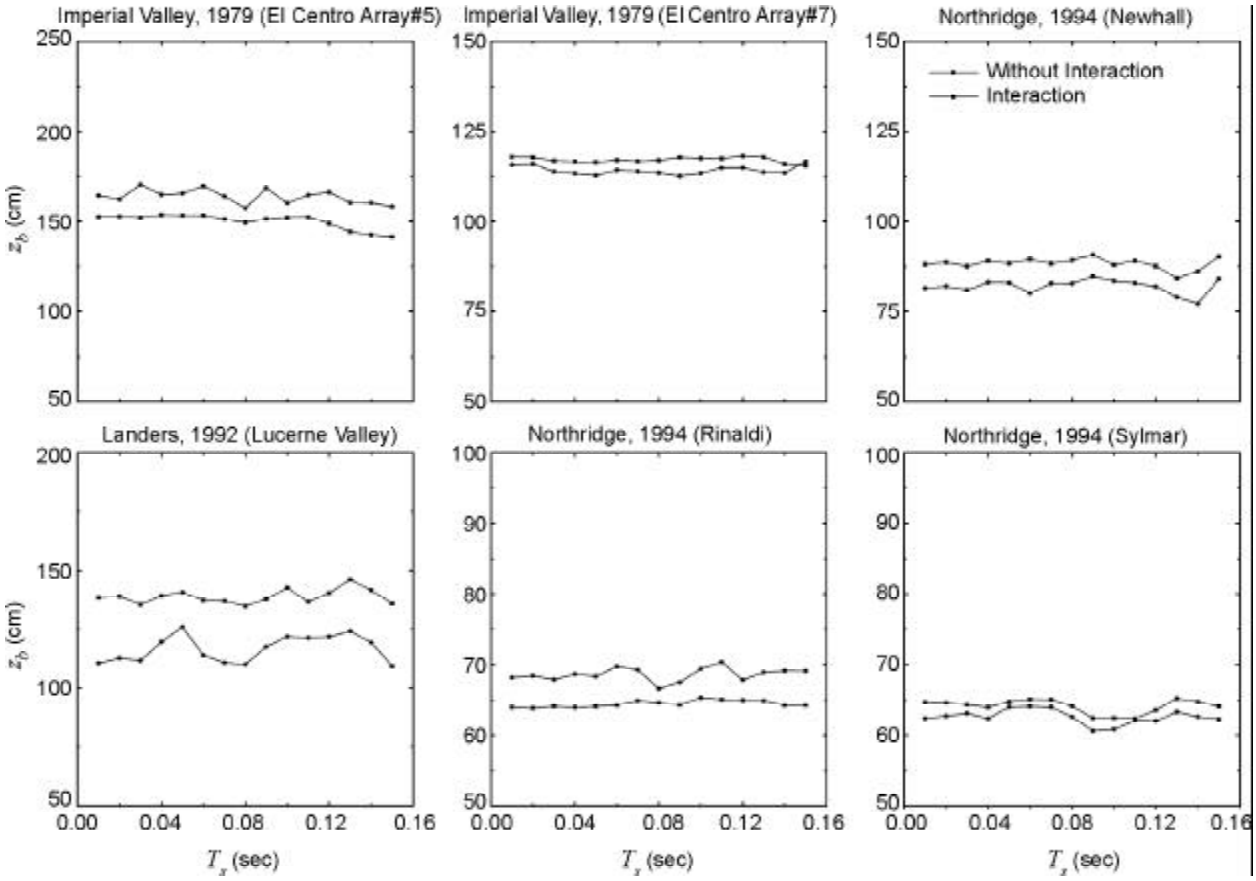

Figure 15. Plot of peak isolator displacement, z_b, of five-story building isolated with the VFPI against the fundamental time period of the superstructure for various near-fault ground motions (considering with and without interaction).

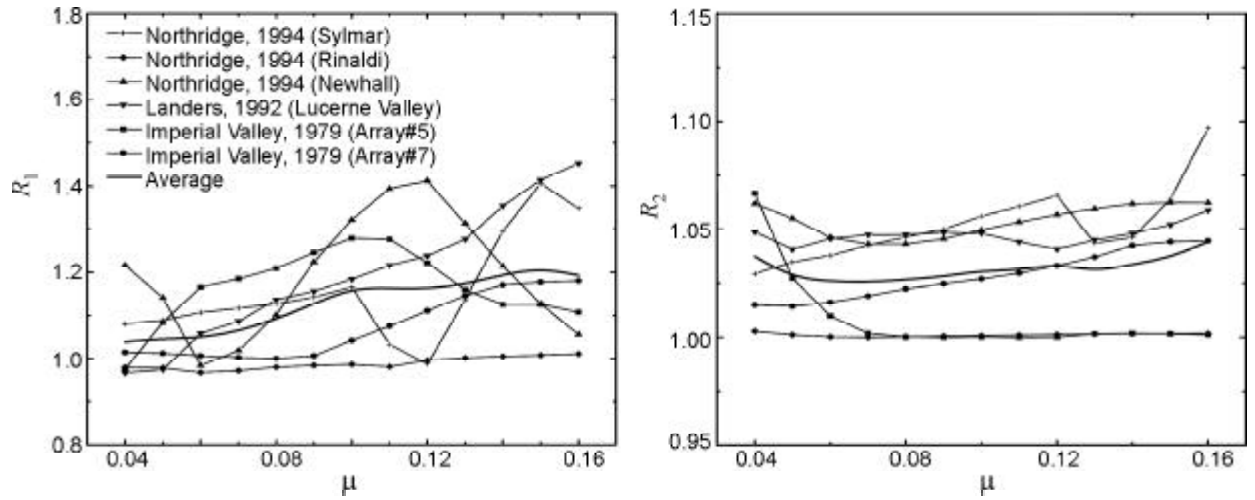

Figure 16. Variation of ratios, R_1 and R_2 against friction coefficient of the VFPI.

interaction effects of frictional forces and values significantly different from unity imply significant interaction effects. On the other hand, values close to unity justify the 2-*D* idealization of the system and the interaction of the frictional forces may be ignored. The ratio, R_1, increases with the increase of friction coefficient of *VFPI*. This indicates that effects of bi-directional interaction increases with the increase in the friction coefficient. In other words, bi-directional interaction effects are relatively less for the low values of the friction coefficient. This is due to the fact that for lower value of friction coefficient, the isolation system remains most of the time in the sliding phase for both cases of excitation (i.e., with and without interaction). As a result, the difference in the sliding displacements for the two cases is relatively less. Moreover, it is found that these effects are strongly dependent on the input ground motions. On the other hand, the R_2 is the ratio of peak resultant isolator displacement, z_b the corresponding peak isolator displacement due to fault normal component, x_b. The ratio, R_2, is not much influenced by the variation of friction coefficient. It varies in the range of 1.026-1.044. This indicated that the resultant isolator displacement of building isolated with *VFPI* under near-fault ground motion may be obtained solely from the normal component, with addition of about 5% to incorporate the contribution from the parallel component. Thus, the contribution of fault parallel component can be neglected in calculating the peak resultant isolator displacement, which is only marginally above the maximum isolator displacement in the fault normal direction.

8. Conclusions

The response of flexible five-story building isolated with the variable frequency pendulum isolator (*VFPI*) under bi-directional near-fault ground motions is investigated using standard numerical technique. The interaction between mobilized frictional forces of the *VFPI* in two horizontal directions is duly incorporated in the governing equations of motion of the building isolated with the *VFPI*. In order to verify the effectiveness of the *VFPI* under bi-directional near-fault ground motions, the seismic responses are compared with that of the same building isolated by the variable friction pendulum system (*VFPS*) and friction pendulum system (*FPS*). The response of the *VFPI*-isolated building with interaction is compared with those without interaction in order to demonstrate the significance of the bi-directional interaction between the mobilized frictional forces of *VFPI*. Furthermore, a parametric study has been carried out to critically examine the influence of important parameters on bi-directional effects of frictional forces of *VFPI*. The important parameters considered are the superstructure time period, frequency variation factor (*FVF*) and friction coefficient of *VFPI*. From the trends of the numerical results of the present study, the following conclusions may be drawn:

- Under bi-directional near-fault ground motions, the isolator displacement in the *VFPI* is more than that of the *VFPS* and the *FPS*, whereas the top floor absolute acceleration and the base shear are less than that of the *VFPS* and the *FPS*.
- The peak isolator displacement of building isolated with the *VFPI* under fault normal and parallel components of near-fault ground motion are found to be more or less uncorrelated.
- The bi-directional interaction of frictional forces has noticeable effects on the response of the building isolated with the *VFPI*. If the interaction of the frictional forces at the sliding interface is ignored, then the superstructure acceleration and base shear will be overestimated and the sliding displacement will be underestimated.
- The resultant maximum isolator displacement of building isolated with the *VFPI* is mainly due to the normal component of the near-fault ground motions. The contribution from the parallel component in the resultant displacement may be ignored. The resultant maximum isolator displacement can be obtained from the fault normal component by increasing about 5% to account the contribution of the parallel component.
- Under near-fault ground motions, the effects of bi-directional interaction of friction forces of the *VFPI* increase with the increase in the friction coefficient.

References

1. Hall, J.F., Heaton, T.H., Halling, M.W., and Wald, D.J. (1995). "Near-Source Ground Motion and Its Effects on Flexible Buildings", *Earthquake Spectra*, **11**, 569-605.

2. Heaton, T.H., Hall, J.F., Wald, D.J., and Halling,

M.W. (1995). "Response of High-Rise and Base-Isolated Buildings to a Hypothetical Mw7.0 Blind Thrust Earthquake", *Science*, **267**, 206-211.

3. Tena-Colunga, A. (1996). "Some Retrofit Options for the Seismic Upgrading of Old Low-Rise School Buildings in Mexico", *Earthquake Spectra*, **12**, 883-902.

4. Tena-Colunga, A., Gomez-Soberon, C., and Munoz-Loustaunau, A. (1997). "Seismic Isolation of Buildings Subjected to Typical Subduction Earthquake Motions for the Mexican Pacific Coast", *Earthquake Spectra*, **13**, 505-532.

5. Jangid, R.S. and Kelly, J.M. (2001). "Base Isolation for Near-Fault Motions", *Earthquake Engineering and Structural Dynamics*, **30**, 691-707.

6. Uniform Building Code (1997). Earthquake Regulations for Seismic Isolated Structures, *International Conf. of Building Officials*, Whittier, CA.

7. Zhou, Q., Lu, X., Wang, Q., Feng, D., and Yao, Q. (1998). "Dynamic Analysis on Structures Base-Isolated by a Ball System with Restoring Property", *Earthquake Engineering and Structural Dynamics*, **27**, 773-791.

8. Hamidi, N., El Naggar, M.H., Vafai, A., and Ahmadi, G. (2003). "Seismic Isolation of Buildings with Sliding Concave Foundation (SCF)", *Earthquake Engineering and Structural Dynamics*, **32**, 15-29.

9. Tsai, C.S., Chiang, T.-C., and Chen, B.-J. (2005). "Experimental Evaluation of Piecewise Exact Solution for Predicting Seismic Responses of Spherical Sliding Type Isolated Structures", *Earthquake Engineering and Structural Dynamics*, **34**, 1027-1046.

10. Tsai, C.S., Chiang, T.-C., and Chen, B.-J. (2003). "Finite Element Formulations and Theoretical Study for Variable Curvature Friction Pendulum System", *Engineering Structures*, **25**, 1719-1730.

11. Murnal, P. and Sinha, R. (2004). "Aseismic Design of Structure-Equipment Systems Using Variable Frequency Pendulum Isolator", *Nuclear Engineering and Design*, **231**, 129-139.

12. Panchal, V.R. and Jangid, R.S. (2008). "Variable Friction Pendulum System for Near-Fault Ground Motions", *Structural Control and Health Monitoring*, **15**, 568-584.

13. Panchal, V.R. and Jangid R.S. (2009). "Seismic Response of Structures with Variable Friction Pendulum System", *Journal of Earthquake Engineering*, **13**, 193-216.

14. Panchal, V.R. and Jangid, R.S. (2008). "Seismic Behavior of Variable Frequency Pendulum Isolator", *Earthquake Engineering and Engineering Vibration*, **7**, 193-205.

15. Jangid, R.S. (1996). "Seismic Response of Sliding Structures to Bi-Directional Earthquake Excitation", *Earthquake Engineering and Structural Dynamics*, **25**, 1301-1306.

16. Jangid, R.S. (1997). "Response of Pure-Friction Sliding Structures to Bi-Directional Harmonic Ground Motion", *Engineering Structures*, **19**, 97-104.

17. Jangid, R.S. (2001). "Response of Sliding Structures to Bi-Directional Excitation", *Journal of Sound and Vibration*, **243**, 929-944.

18. Matsagar, V.A. and Jangid, R.S. (2006). "Seismic Response of Simply Supported Base-Isolated Bridge with Different Isolators", *International Journal of Applied Science and Engineering*, **4**, 53-69.

19. Rao, P.B. and Jangid, R.S. (2001). "Performance of Sliding Systems under Near-Fault Motions", *Nuclear Engr. and Design*, **203**, 259-272.

20. Pranesh, M. and Sinha, R. (2000). "VFPI: An Isolation Device for Aseismic Design", *Earthquake Engineering and Structural Dynamics*, **29**, 603-627.

21. Constantinou, M.C., Mokha, A.S., and Reinhorn, A.M. (1990). "Teflon Bearing in Base Isolation II: Modeling", *J. of Structural Engineering, ASCE*, **116**, 455-474.

22. Mokha, A., Constantinou, M.C., and Reinhorn, A.M. (1993). "Verification of Friction Model of Teflon Bearings under Triaxial Load", *J. of Structural Engineering, ASCE*, **119**, 240-261.